Far-field second-harmonic fingerprint of twinning in single ZnO rods

S. W. Liu,[1] H. J. Zhou,[2] A. Ricca,[1] R. Tian,[2] and Min Xiao[1]
[1]*Department of Physics, University of Arkansas, Fayetteville, Arkansas 72701, USA*
[2]*Department of Chemistry and Biochemistry, University of Arkansas, Fayetteville, Arkansas 72701, USA*
(Received 30 November 2007; published 24 March 2008)

The third-rank susceptibility tensor that describes the second-harmonic generation changes sign after an inversion operation indicating its sensitivity to twinning structures. Here, we show the far-field scattering patterns of second-harmonic (SH) radiation generated by single twinned and twin-free ZnO rods. The patterns have been successfully correlated with the twinning structures. A finite dipole-wire model has been effectively employed to model the pattern. It indicates that the dark or bright fringes at the 0° scattering angle originate as a result of the destructive or constructive interference of SH waves emitted from each halves of the twinned or twin-free ZnO rod.

DOI: 10.1103/PhysRevB.77.113311 PACS number(s): 61.46.Hk, 42.65.Ky, 61.72.Mm, 78.67.Bf

So far, studies on the optical properties of zinc oxide (ZnO) nanostructures[1–5] have mainly focused on the near ultraviolet (NUV) photoluminescence. Some advanced nanophotonic devices, such as NUV nanolaser,[6] photodetector, and optical switches,[7] have been demonstrated based on ZnO nanowires. However, as a nonlinear optical material, the second-order nonlinear optical properties of ZnO nanostructures, such as second-harmonic generation (SHG),[8–10] were not fully exploited. Currently, the second-harmonic (SH) measurements on single semiconductor nanostructures focus on the SH images and polarization diagrams of single nanowires in reflection geometry.[8,10] No attention has been paid to the SH scattering patterns because the pattern is difficult to observe in these experimental configurations. In addition, crystal twinning is a common feature in many ZnO nanostructures,[11–14] but its effects on the optical properties of ZnO nanostructures have not been investigated so far. Actually, SH scattering patterns include more information about the SH wave, such as the phase, than simple SH images or polarization diagrams. The scattering patterns are found to be closely associated with the polarity inside the ZnO nanostructures.

In this Brief Report, we present our observation of the far-field scattering patterns of the transmitted SH waves from single twinned and twin-free ZnO rods. More interestingly, the distribution of the interference fringes in the scattering pattern is directly related to the twinning structures inside the rods. A simple model based on the radiation from finite dipole wires has been developed to simulate the experimentally measured scattering patterns and highlight the different features of the zero-angle fringes between two kinds of rods. The dark or bright fringes at the 0° scattering angle would be attributed to destructive or constructive interferences of the SH electromagnetic waves emitted from each halve of the twinned or twin-free rods.

The ZnO rods were grown on fused quartz with the aqueous solution method. The polar axes of rods are parallel to the surface of fused quartz with the length of several micrometers and diameter of 100–250 nm. The SH radiation is generated using a mode-locked Ti:sapphire laser (Tsunami) pumped by Millenia Xs continuous-wave laser (Spectra Physics), producing 100 fs laser pulses centered at approximately 810 nm with a repetition rate of 82 MHz. The transmitted SH signals were measured under normal incidence with the polarization direction along the rod's axis. Figure 1(a) is a typical SH image for a single rod with the length of 3.8 μm. The image exhibits the strong far-field scattering fringes resulting from the interferences of the SH waves emitted from the different locations along the axis of the rod. The number of the interference fringes decreases as the length of the rod is reduced, as shown in Fig. 1(b) for a shorter rod with the length of 1.5 μm. The insets are the enlarged images of the rods with their brightness reduced to view the detailed information clearly. It is obvious that a small dark gap with low SHG efficiency exists at the center

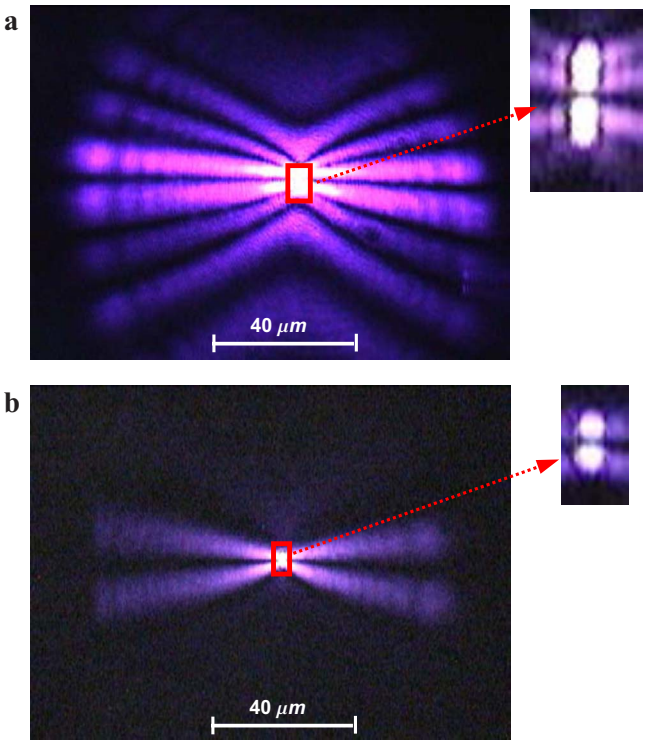

FIG. 1. (Color online) SH images and scattering patterns for single twinned ZnO rods. The insets show the enlarged SH images for the twinned ZnO rods. (a) ZnO rod with the length of 3.8 μm. (b) ZnO rod with the length of 1.5 μm.

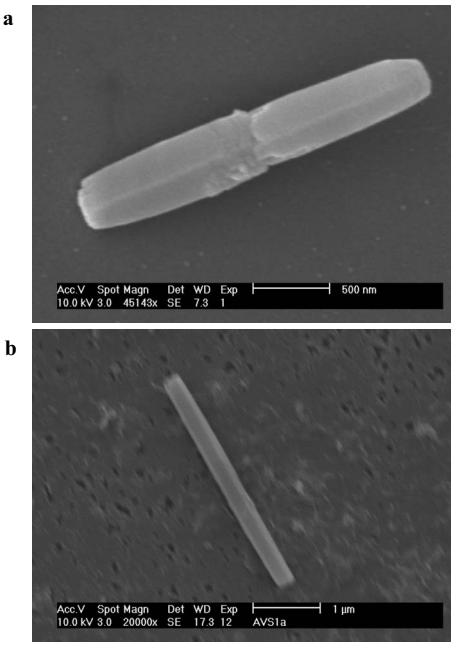

FIG. 2. SEM images of two typical ZnO rods. (a) ZnO rod with the twinning structure. Higher resolution is used to see the twinning interface at the center. (b) ZnO rod without the twinning structure.

of both rods. A dark fringe, which neighbors with two brightest fringes, extends out from the dark gap at a scattering angle of 0°. This feature is much clearer for the shorter rod, where the fringes at higher scattering angles are invisible and the two brightest fringes scatter at a larger angle [Fig. 1(b)]. The scanning electron microscopy (SEM) image, as shown in Fig. 2(a), reveals that the rod is bisected into halves by a special interface structure at the center, with respect to the SEM image, as shown in Fig. 2(b), for a typical twin-free rod. Some authors have described this kind of structures as the dumbbell-shaped bicrystals that are bisected by a central (0001) twinning plane. The polarity is thus likely pointed away from the terminal surface toward the central (0001) twinning plane.[11] Because the third-rank susceptibility tensors (χ_{ijk}) for the two twinned crystals have an opposite sign, the SH waves generated from them will be out of phase by 180° at the scattering angle of 0°. Their destructive interferences always lead to a dark fringe. A rigorous treatment for this problem has to resort to the enormous numerical analysis for the linear and second-order light scattering by a finite twinned hexagonal rod on a substrate. However, considering that the average distribution of the SH intensity in the image exhibits a feature of dipole radiation, we simplify the rod to a finite bisected wire that has a uniform density of electric dipole sources directing to the wire's axial directions but with the two segments oscillating out of phase by 180° at the SH frequency. The effective electric dipole sources are attributed to the nonlinear polarization $P^{2\omega}$ that is excited by the fundamental field E^{ω} ($P^{2\omega}=\chi_{ijk}:E^{\omega}E^{\omega}$). In particular, under our polarization configuration, only axial component of the nonlinear polarization is excited via $P_3^{2\omega}=\chi_{333}(E_3^{2\omega})^2$, where 3 refers to the polar axis. Actually, SH polarization diagrams[8,10] have been measured, which were well explained by the nonlinear susceptibility tensor (χ_{ijk}) under the symmetry group (6 mm) of ZnO lattice with its polar direction along the rod's axis. Our assumption is similar to the quasistatic approximation[10] but takes the finite length of rods to be considered. Here, we want to emphasize that the coherent length for the SH back irradiation is at least 1 order less than that for the forward-irradiating (transmitted) SH signal in ZnO at our wavelength. In addition, the reflection of the SH back-irradiating signal at the interface between the ZnO and fused quartz is also low (4% for intensity). Therefore, the SH back irradiation collected in our experimental geometry is much weaker (at least 2 orders less) than the forward-irradiating SH signal. The presence of the fused quartz substrate can thus be neglected. We found that many of the image's features can be explained by this model of finite dipole wire without losing important physics.

As shown in Fig. 3(a), the two segments of the bisected dipole wire are assumed to have an opposite polarity labeled by two opposite blue arrows directing to $\pm y'$ axes, respectively. Therefore, the z component $S_z^{2\omega}$ of the time-average Poynting vector at a point (x,y) of the image plane, which is away from the dipole wire by an effective distance d_{eff}, can be approximately written as

$$S_z^{2\omega}(x,y,d_{eff}) = -\frac{1}{2\mu_\circ}\mathrm{Re}\left[\int_{-L/2}^{L/2} E_z^{2\omega}(x,y,d_{eff},y')^* dy' \times \int_{-L/2}^{L/2} B_y^{2\omega}(x,y,d_{eff},y')dy'\right], \quad (1)$$

where the wire extends from $y'=-L/2$ to $y'=L/2$ along the y' axis; $E_z^{2\omega}$ and $B_y^{2\omega}$ are the corresponding components of the SH electric and magnetic fields in the image plane, which are generated by a unit length of electric dipole distributed along the y' axis. The fields take on the following forms:[15]

$$E_z^{2\omega} \sim \pm[\sin^2\theta + (3\cos^2\theta - 1)(1/r^2 - 2i\omega/c/r)/(2\omega/c)^2]e^{i2\omega/cr}/r, \quad (2)$$

$$B_y^{2\omega} \sim \pm \sin\theta\cos\phi[c/(2i\omega r) - 1]e^{i2\omega/cr}/r, \quad (3)$$

where $\pm$ signs are chosen according to the two integration spans [plus for $(-L/2,0)$ and minus for $(0,L/2)$], which represent the positive and negative polarities of the two segments of the bisected dipole wire, and

$$r = [x^2 + (y-y')^2 + d_{eff}^2]^{1/2},$$

$$\sin^2\theta = (x^2 + d_{eff}^2)/[x^2 + (y-y')^2 + d_{eff}^2],$$

$$\cos^2\phi = d_{eff}^2/(x^2 + d_{eff}^2),$$

where d_{eff} is taken as a small parameter to optimize the simulation. It may be caused by the finite diameter of the rod, or the finite depth of field of the objective, or the incomplete treatment due to our approximation.

Figure 3(b) is a density plot of $S_z^{2\omega}(x,y,d_{eff})$ for a bisected dipole wire with the same length as the rod in Fig. 1(a). The simulation with d_{eff} taken as 20.25 μm exhibits a very similar distribution of the interference fringes as Fig. 1(a). Also,

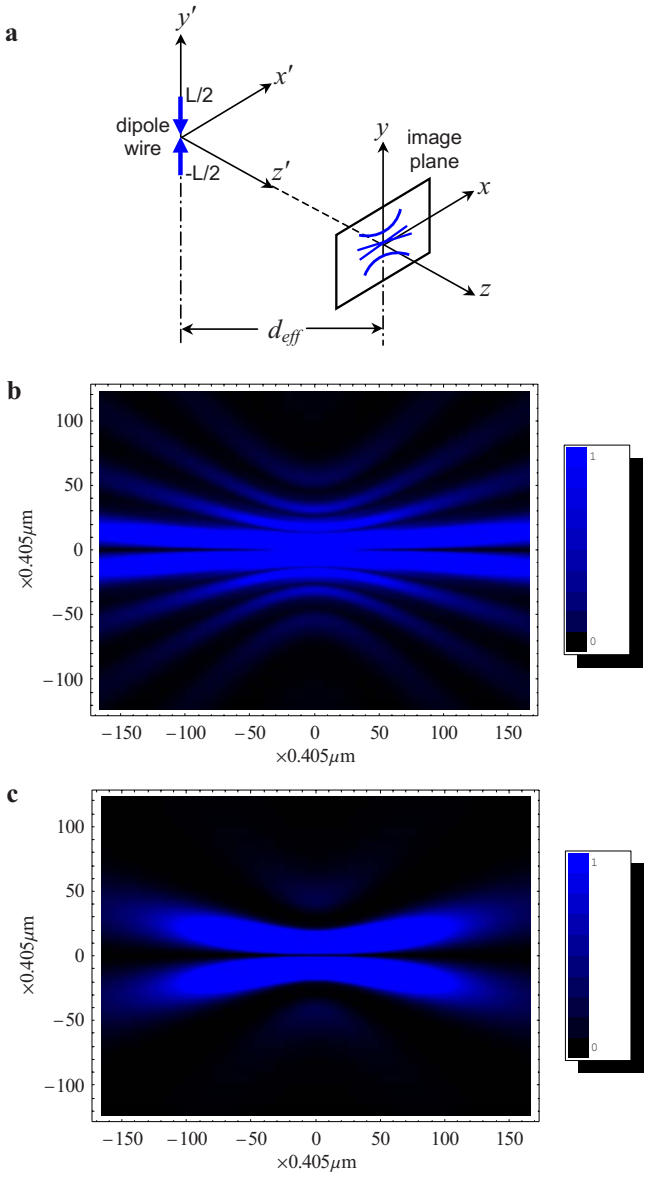

FIG. 3. (Color online) Theoretical analysis of the interference fringes in the SH images of twinned ZnO rods. (a) Calculation geometry by simplifying the twinned rod to a finite bisected dipole wire. The dipole wire has a finite length L and a uniform dipole density, but an opposite polarity on the positive and negative y' axis. The dipole wire is away from the image plane (xy plane) by an effective distance d_{eff}. (b) Numerical simulation of the z component of the time-average Poynting vector on the image plane for a twinned rod with the length of 3.8 μm. (c) Numerical simulation of the z component of the time-average Poynting vector on the image plane for a twinned rod with the length of 1.5 μm.

as expected, the dark fringe appears at the zero scattering angle in the simulation. Figure 3(c) is another simulation with d_{eff} taken as 16.2 μm for the shorter rod in Fig. 1(b). The simulation exhibits a smaller number of fringes, a much wider dark fringe at the scattering angle of 0°, and a larger scattering angle for the two brightest fringes, which well agree with the experiment. To illuminate that the dark fringe is a unique feature of the twinned rod, we measured the

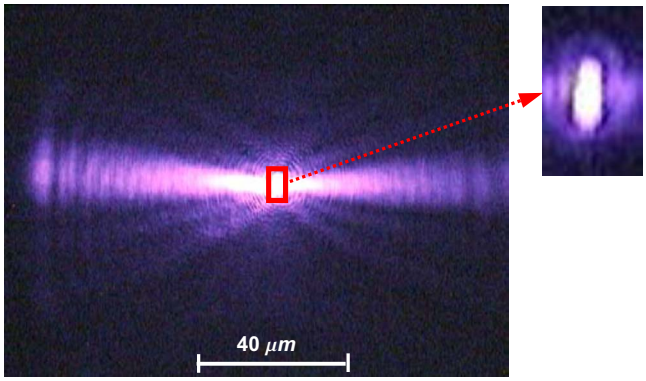

FIG. 4. (Color online) SH image and scattering pattern for a single twin-free ZnO rod with the length of 1.5 μm. The inset shows an enlarged SH image of the twin-free ZnO rod.

far-field SH scattering pattern (Fig. 4) from a single twin-free rod with the same length as the twinned rod in Fig. 1(b). It shows a very wide bright fringe at the scattering angle of 0°. No dark gap is observed in the enlarged image, as shown in the inset of Fig. 4. The bright fringe results from the constructive interference of the SH waves radiated by the nonlinear polarization oscillating in phase at every point along

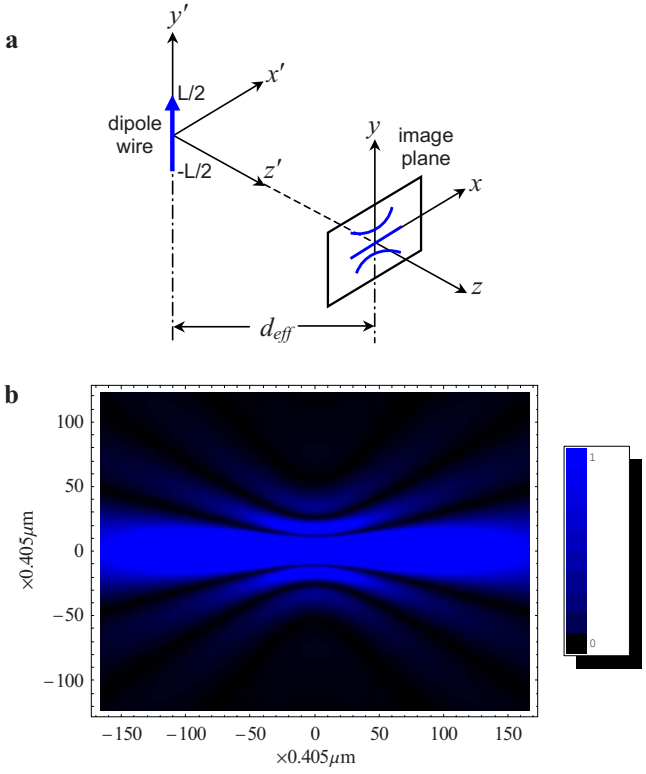

FIG. 5. (Color online) Theoretical analysis of the interference fringes in the SH image of twin-free ZnO rod. a, Calculation geometry by simplifying the twin-free rod to a finite dipole wire with polarity directing to positive y' axis and extending from $y'=-L/2$ to $y'=L/2$. The dipole wire is away from the image plane by an effective distance d_{eff}. (b) Numerical simulation of the z component of the time-average Poynting vector on the image plane for a twin-free rod with the length of 1.5 μm.

the twin-free rod. The twin-free rod is modeled by a finite dipole wire with polarity directing to positive y' axis, as shown in Fig. 5(a). The theoretical simulation in this case is realized by omitting $\pm$ signs in Eqs. (2) and (3) and computing Eq. (1). As shown in Fig. 5(b), the simulation with d_{eff} taken as 16.2 μm well agrees with the measured pattern in Fig. 4.

In summary, we observed the SH far-field scattering patterns from single twinned and twin-free ZnO rods. The distributions of the interference fringes in the pattern have been successfully correlated with the twinning structure in the rods. The fringe at the scattering angle of 0° is dark for the twinned rod due to the destructive interference, but bright for the twin-free rod due to the constructive interference. A theoretical model based on the radiation from finite dipole wires has been successfully employed to simulate the patterns for both kinds of rods. Also, the SH scattering pattern extends the applications of SHG in probing crystalline orientation and homogeneity.[16] It offers a very convenient, noncontact, and *in situ* tool to monitor the twinning structure in rods. The SH scattering patterns distribute in a large area and are thus very easy to be observed without high-resolution microscope. Through this work, it is possible, in principle, for the researchers to identify the polarities in more complicated ZnO nanostructures by the SH scattering patterns.

The work in the Physics Department is partially supported by grants from the Army Research Laboratory (DAAD19-03-2-0017) and the Army Research Office (W911NF-05-1-0353). The work in the Chemistry/Biochemistry Department is partially supported by the University of Arkansas, Arkansas Bioscience Institute, and NSF-MRSEC; A.R. is supported via MicroEP REU program in the Physics Department.

[1] Y. Huang, X. Duan, Q. Wei, and C. M. Lieber, Science **291**, 630 (2001).
[2] P. Yang, H. Yan, S. Mao, R. Russo, J. Johnson, R. Saykally, N. Morris, J. Pham, R. He, and H. J. Choi, Adv. Funct. Mater. **12**, 323 (2002).
[3] Z. W. Pan, Z. R. Dai, and Z. L. Wang, Science **291**, 1947 (2001).
[4] Z. R. Tian, J. A. Voigt, J. Liu, B. Mckenzie, M. J. Mcdermott, M. A. Rodriguez, H. Konishi, and H. F. Xu, Nat. Mater. **2**, 821 (2003).
[5] P. X. Gao, Y. Ding, W. Mai, W. L. Hughes, C. Lao, and Z. L. Wang, Science **309**, 1700 (2005).
[6] M. H. Huang, S. Mao, H. Feick, H. Yan, Y. Wu, H. Kind, E. Weber, R. Russo, and P. Yang, Science **292**, 1897 (2001).
[7] H. Kind, H. Yan, B. Messer, M. Law, and P. Yang, Adv. Mater. (Weinheim, Ger.) **14**, 158 (2002).
[8] J. C. Johnson, H. Yan, R. D. Schaller, P. B. Petersen, P. Yang, and R. J. Saykally, Nano Lett. **2**, 279 (2002).
[9] R. Prasanth, L. K. V. Vugt, D. A. M. Vanmaekelbergh, and H. C. Gerritsen, Appl. Phys. Lett. **88**, 181501 (2006).
[10] J. P. Long, B. S. Simpkins, D. J. Rowenhorst, and P. E. Pehrsson, Nano Lett. **7**, 831 (2007).
[11] T. L. Sounart, J. Liu, J. A. Voigt, J. W. P. Hsu, E. D. Spoerke, R. Tian, and Y. Jiang, Adv. Funct. Mater. **16**, 335 (2006).
[12] B. G. Wang, E. W. Shi, and W. Z. Zhong, Cryst. Res. Technol. **33**, 937 (1998).
[13] Y. Dai, Y. Zhang, Y. Q. Bai, and Z. L. Wang, Chem. Phys. Lett. **375**, 96 (2003).
[14] Y. Dai, Y. Zhang, and Z. L. Wang, Solid State Commun. **126**, 629 (2003).
[15] J. D. Jackson, *Classical Electrodynamics* (Wiley, New York, 1999).
[16] L. Mahieu-Williame, S. Gresillon, M. Cuniot-Ponsard, and C. Boccara, J. Appl. Phys. **101**, 083111 (2007).